cytoplasmic inclusions (GCIs) in MSA [32, 34, 39]. MSA is a sporadic neurodegenerative disease characterized clinically by varying degrees of parkinsonism, cerebellar ataxia and autonomic dysfunction and pathologically by degeneration in the substantia nigra, putamen, inferior olivary nucleus, pontine nuclei and cerebellum [26]. In addition to neuronal loss in these selective areas, iron pigment accumulation, gliosis and myelin pathology are increasingly recognized. In affected areas, myelin displays signs of degeneration and oligodendroglia contain argyrophilic inclusion bodies called GCIs [21, 23, 27]. GCIs are composed of coated filaments with a diameter of 10–15 nm that are immunoreactive for ubiquitin (Ub) and αS. Because GCI is a pathological hallmark of MSA, numerous studies have tried to find possible correlations between appearance of GCIs and degeneration, which, however, have failed to demonstrate any (either positive or negative) correlation. Instead, occurrence of GCIs seems rather capricious in their quantity. For example, they could be abundant in early cases or where degeneration remains slight as in the motor cortex [15, 17]. One of the difficulties may be related to the fact that GCIs, as well as LBs and other pathological inclusions, are composed of multiple proteins that possibly interact with each other during or after formation of these inclusions. This prompted us to examine different epitopes or staining features in each GCI to identify possible evolutionary changes by quantifying and comparing GCIs from different brain regions from patients with different disease duration. It is possible that a relation between epitopes rather than a representation of a single epitope itself is more closely related to evolutionary changes as we demonstrated on LBs in the previous study [29]. To avoid possible ambiguity on fluorescence signals that are sometimes cumbersome, we used dual enhancement of double immunofluorescence signals by CARD, as we have established recently [35, 37], which enabled immunofluorescence signals from αS and Ub to be quantified precisely. Simultaneous detection of thiazin red (TR) signal from the same structure provided additional information, possibly related to fibrillary status of each GCI under observation [36]. Moreover, identification of each GCI on subsequent Gallyas silver staining [3] confirmed the authenticity of GCI in these areas. Quantification of over 1,600 GCIs for these staining profiles clarified their possible relation to disease progression.

Materials and methods

Four patients with the clinicopathological diagnosis of MSA (three male/one females; age at death, range 47–74 years), autopsied at the Department of Pathology, Tokyo Metropolitan Neurological Hospital, Tokyo, Japan, were enrolled in this study. Duration of the disease ranged from 4 to 15 years. Clinical diagnosis of MSA was confirmed postmortem on the basis of neuronal loss and the presence of GCIs in the relevant regions including the putamen, cerebellar white matter, and motor cortex. Formalin-fixed, paraffin-embedded blocks were sampled from the putamen, cerebellar white matter and motor cortex. Sections were deparaffinized after cutting at 4 μm. To observe localization of the two epitopes (αS and Ub) more clearly without cross-talk, each fluorescence signal from the two epitopes was amplified as described previously as dual enhancement of double immunofluorescence signals by CARD [35, 37]. Briefly, after treatment with 2% H_2O_2 to inactivate endogenous peroxidases, sections were incubated for 48 h at 4°C with a monoclonal antibody against αS (LB509 [19], 1:300, courtesy of Prof. Iwatsubo, University of Tokyo, Tokyo, Japan) diluted with 0.01 M phosphate-buffered saline (pH 7.4) containing 0.03% Triton X-100 (PBST) and 5% normal goat serum. Sections were washed for 10 min three times with PBST between the steps throughout the procedure. After incubation with an anti-mouse IgG conjugated with horseradish peroxidase (HRP, 1:500, Kirkegaard and Perry, Gaithersburg, MD) for 2 h, the HRP signal was directly visualized with FITC-conjugated tyramide (FITC-tyramide, 1:200, NEN Life Science Products, Boston, MA) in the dark. Next, HRP was again blocked by incubating the section with 2% H_2O_2 in 0.1 M Tris-buffered saline for 30 min. The sections were then incubated with a rabbit polyclonal antibody against Ub (Z0458, 1:500, Dako, Glostrup, Denmark) at 4°C for 48 h. After incubation with an anti-rabbit IgG conjugated with HRP (HRP, 1:500, Pierce, Rockford, IL) for 2 h, the HRP signal was enhanced by reaction of biotinylated tyramide [1] (1:1,000) for 10 min. The amplified signal was visualized with Cy5-conjugated streptavidin (Cy 5-labeled streptavidin, 1:200, Kirkegaard and Perry). After washing, stained sections were then immersed in 0.01 M PBS containing TR (1:30,000, Wako, Tokyo, Japan) for 30 min. After washing, they were mounted with buffered glycerol containing *p*-phenylenediamine to minimize photobleaching. Sections were observed under a fluorescence microscope combined with laser confocal system (TCS-SP, Leica, Heidelberg, Germany). This system is equipped with spectrophotometer consisting of a prism and two sets of movable slit in front of the detection photomultiplier, which select arbitrarily whatever wavelength between 400–800 nm for the light path to be detected. For balanced excitation of fluorochromes, an Ar-Kr laser is combined with acousto-optical tunable filter system, which enables the individual intensity of each of the three laser beams (488 nm, 568 nm and 647 nm) to be adjusted independently. FITC, which labels the αS epitope, was excited by the 488 nm beam and was detected through a light path of the range 500–540 nm. Cy5, which labels the Ub epitope, was excited by the 647 nm beam and was detected through a light path at 690–730 nm. TR (emission peak: 620 nm) was excited by the 568 nm beam and was detected through a light path at 600–640 nm. After triple-stained images were photographed

and recorded on magneto-optical disks, the same section was stained with Gallyas silver stain [3], a silver staining highly sensitive in detecting GCIs. This series of procedure enabled the relationship between four different staining features, αS-like immunoreactivity (IR), Ub-like IR, TR positivity and argyrophilia by Gallyas silver stain to be assessed on each GCI. At least one hundred GCIs on each section from the putamen, cerebellar white matter, and motor cortex from each case were classified according to their staining profiles into four categories; αS + Ub–: αS positive and Ub negative; αS + Ub + : positive for both αS and Ub; αS–Ub + : αS negative and Ub positive; αS–Ub–: negative for both αS and Ub. In total, 1,690 GCIs were examined for their staining profiles.

Because the frequency of GCIs was highly variable, we calculated, for statistical analyses, GCI number (total number of GCIs/number of microscopic fields) for each individual area examined. The GCI numbers were subdivided according to four different staining profiles (profile number: number of GCIs with one of the four staining profiles/microscopic field for each individual area). The sum of the profile numbers from the three areas (putamen, cerebellar white matter and motor cortex) of each case were calculated to represent the profile of the case (case-profile number) and used for chi-square analysis. Case-profile numbers for each case were also transformed into % fractions to represent the "% case-profile" of the case. Because the four cases were highly variable in disease duration, regression analysis was performed between the disease duration and the % case-profile.

Profile numbers from the same area of the four cases were also assembled to represent the profile of each area (area-profile number). Based on the area-profile numbers, regional differences were assessed also on contingency table (chi-square analysis). Area-profile numbers for each area were also transformed into % fractions to represent "% area-profile". Severity of degeneration was assessed on hematoxylin-eosin stained sections and classified as mild, moderate or severe, according to the degree of cell loss and/or gliosis and loss of myelin [27].

Results

Dual enhancement of two different fluorescent signals was successful in detecting highly intense signals from αS (FITC) and from Ub (Cy5) without cross-talk between the TR signal. Because the same section was subjected to the Gallyas silver stain, the same GCI already recorded as multi-labeled fluorescence images, was identified on the same section stained with Gallyas silver method to assure that the Gallyas-positive inclusions were nothing but GCIs. Structures lacking argyrophilia were immunopositive neither for αS nor for Ub. All the four cases were diverse in either age at

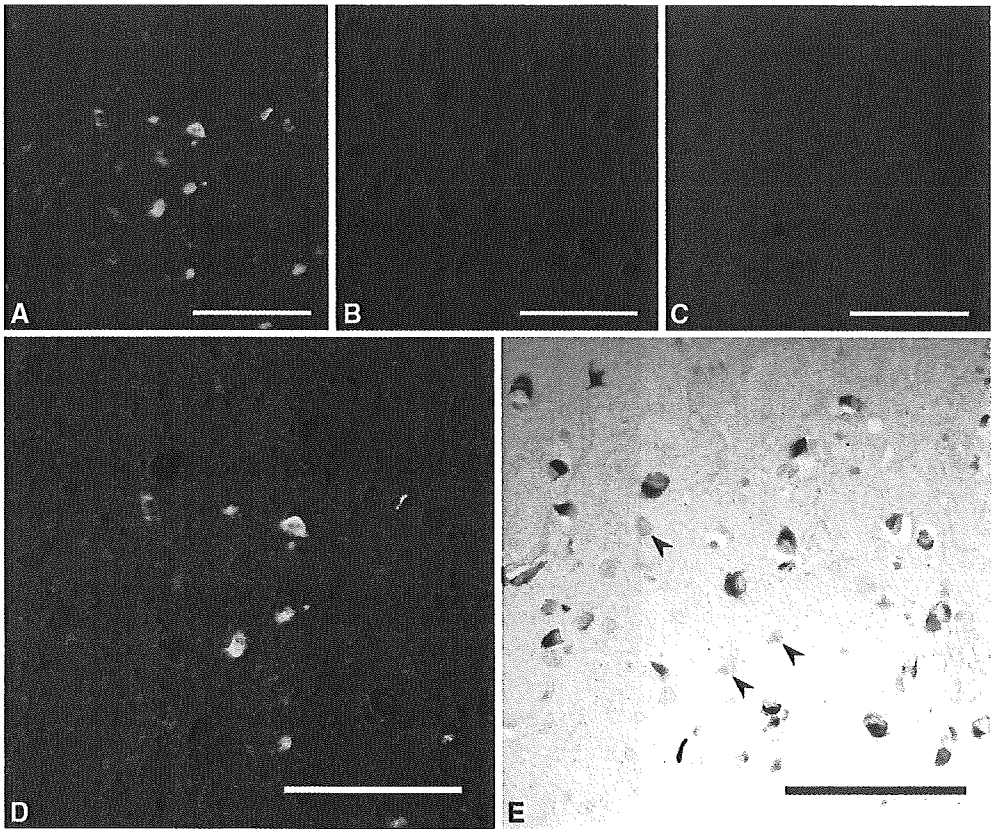

Fig. 1 Multi-fluorolabeling of GCIs (A–D) for αS (**A**, *green*), Ub (**B**, *blue*) and TR (**C**, *red*) and their merged image (**D**). After recording these fluorescence images, each section was subsequently stained with Gallyas silver method, and the same microscopic field was identified to examine staining profiles of Gallyas-positive GCIs (**E**). Although the staining profile of each GCI is heterogeneous, affinity to TR is consistently absent (**C**). Round fluorescent structures were consistently stained with Gallyas silver stain and identified as GCIs. Faint Gallyas silver staining not accompanied by fluorescent signals (*arrowheads* in **E**) were considered not to be GCIs and excluded from quantification (*GCI* glial cytoplasmic inclusion, αS α-synuclein, *Ub* ubiquitin, *TR* thiazin red). *Bars* 100 μm

death, duration of the disease, or severity of tissue degeneration. Irrespective of this heterogeneity, all of the GCIs lacked affinity to TR without exception. Contrarily, αS-like IR and Ub-like IR were heterogeneous (Figs. 1, 2). The density of GCI in each area did not correlate with the severity of tissue degeneration (Fig. 3). For example, mild degeneration of motor cortex seen in case 1 with the shortest duration (4 years) was accompanied by a few GCIs (7.2/mm^2), while moderate degeneration of cerebellar white matter was associated with a large number of GCIs (55.2–95.2/mm^2) in cases 2, 3 and 4.

Chi-square analyses based on the case-profile numbers were performed initially with a whole contingency table (case-profile numbers × cases 1–4) and demonstrated a significant difference ($P < 0.0001$) in the profiles between the cases. Figure 4 shows the % case-profile (% fraction calculated based on the numbers of GCIs with different profile from each case) of GCI in relation to the disease duration and demonstrated an apparent increase in αS–Ub+ GCIs and an apparent decrease in αS+Ub+ GCIs along the disease duration. This trend was confirmed by detailed chi-square analyses on these case-profile numbers, as follows. The number of αS–Ub+ GCIs was significantly different between cases 4 and 3 ($P < 0.0001$, Fig. 4), and between cases 3 and 2 ($P < 0.0001$, Fig. 4). The number of αS+Ub+ GCIs was also significantly different between cases 1 and 2 ($P < 0.0001$, Fig. 4), and between cases 3 and 4 ($P < 0.0001$, Fig. 4). Comparison of the number of αS+Ub+ GCIs and that of αS–Ub+ GCIs between cases 2 and 3 by Chi-square analysis exhibited no significant difference. The difference was, however, significant between cases 1 and 2 ($P = 0.0008$, Fig. 4), which was attributable to the predominance of αS+Ub+GCIs in case 1. The opposite predominance of αS–Ub+GCIs in case 4 relative to case 3 made this difference again significant ($P = 0.0001$, Fig. 4). Moreover, the prevalence of αS–Ub+ GCIs (% case-profile) exhibited a linear positive correlation with the duration of disease (Fig. 5, $R^2 = 0.983$), while αS+Ub+ GCIs exhibited a reciprocal trend (Fig. 5, $R^2 = 0.752$). All of these statistically significant differences are compatible with the apparent tendency with a progressive increase in αS–Ub+ GCIs and the reciprocal decline in αS+Ub+GCIs along the disease progression.

In addition to these significant differences in staining profile according to cases, its regional difference was also

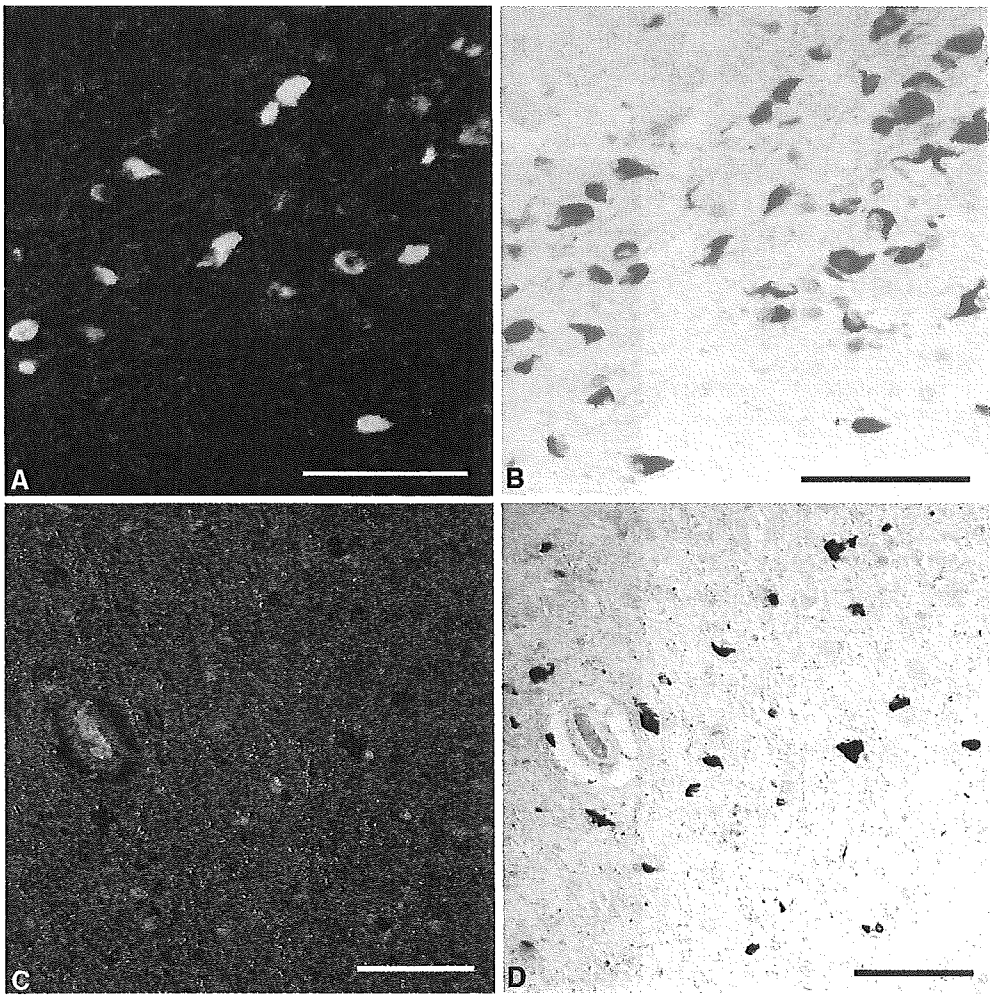

Fig. 2 Heterogeneous staining profiles of GCIs. Examples are the putamen from a case with the shortest duration (4 years, **A**, **B**) and the motor cortex from the longest duration (15 years, **C**, **D**). **A**, **C** Merged images as in Fig. 1. **B**, **D** Gallyas stained image from the same microscopic field as **A**, **C**, respectively. αS+Ub– GCIs are frequent in the putamen with shortest duration (**A**). In contrast, αS–Ub+ GCIs (*blue*) are predominant in the motor cortex with longest duration (**C**), where TR (*red*) and Ub (*blue*) signals are not detectable even when photomultipliers are sensitized to their maximum to yield significant background. *Bars* 50 μm

analyzed. Chi-square analyses based on the area-profile numbers were performed initially with a whole contingency table (area-profile numbers × motor cortex, cerebellar white matter, putamen) and demonstrated a significant difference ($P < 0.0001$) in the profiles between the areas. Detailed chi-square analyses clarified that cerebellar white matter was characterized by a predominance of αS + Ub + GCIs relative to putamen and motor cortex ($P < 0.0001$). In contrast, motor cortex was characterized by a predominance of αS–Ub + GCIs relative to cerebellar white matter ($P = 0.0016$) and to putamen ($P = 0.0002$). Figure 6 shows % area-profile (% fraction calculated based on the numbers of GCIs of the same area from the four cases) different according to areas.

Discussion

GCIs appear in the cerebellar white matter, dorsolateral part of putamen and pons where severe degeneration is observed in MSA. Because they also appear frequently even in other regions where neuronal degeneration is not evident, it is considered that the occurrence of GCIs does not necessarily correlate with the degree of the neuronal degeneration [26] nor the severity of astrocytosis [6]. One of the possibilities is that GCIs may disappear with progression of degeneration [15]. Interpretations claimed by previous studies based on single staining are, however, still highly conflicting [15, 17, 21, 26, 27]. Although αS and Ub are common con-

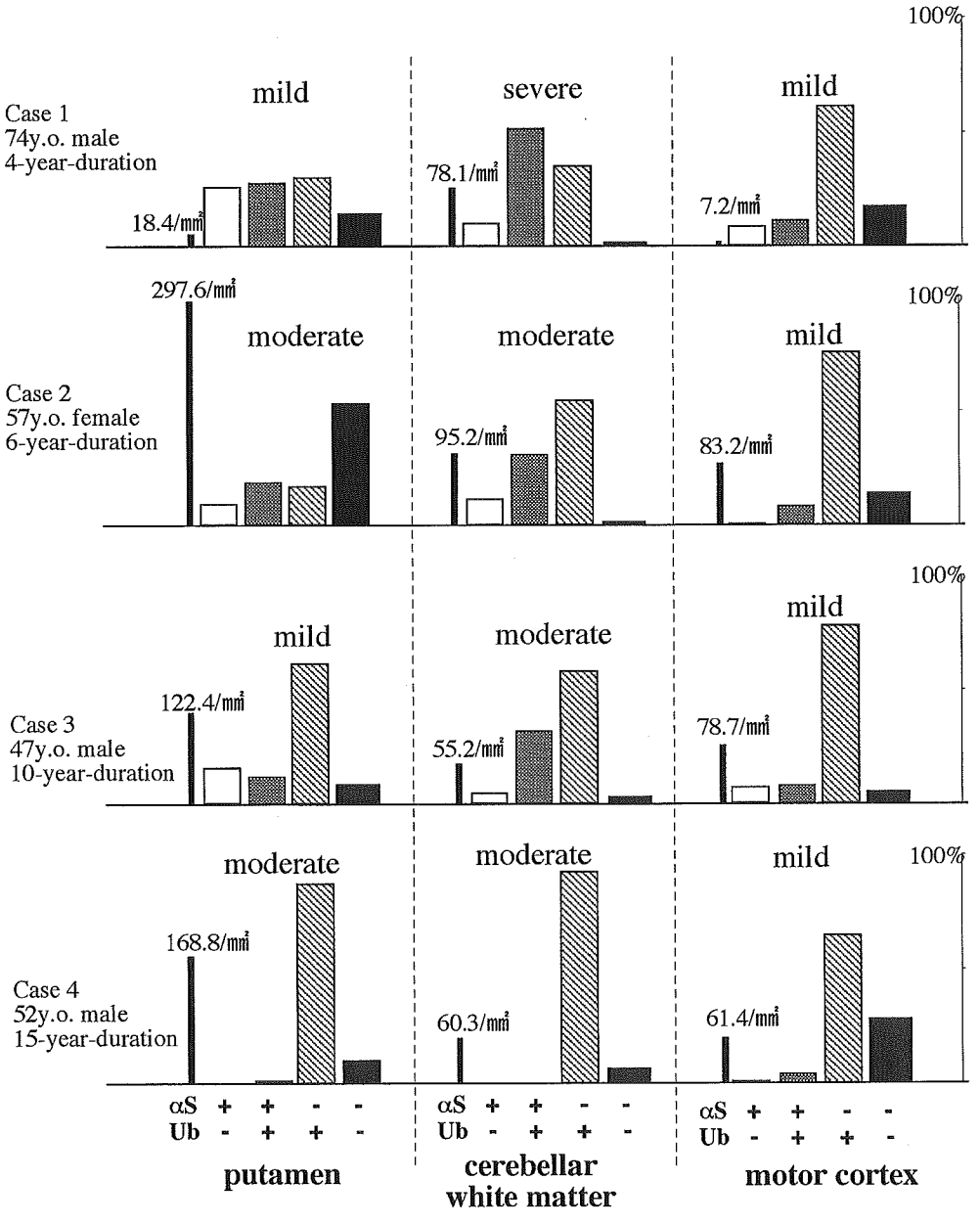

Fig. 3 Density and staining profiles of GCIs in different areas (putamen, cerebellar white matter and motor cortex) from four cases. Cases are arranged from top to bottom with increasing duration of the disease. Staining profiles of GCIs are shown as relative frequency of GCIs stained differently, each represented by different columns as follows; *blank columns*: αS + Ub–; *gray columns*: αS + Ub +; *hatched columns*: αS–Ub +; *black column*: αS–Ub–. All of these GCIs were identified on Gallyas-stained sections after immunofluorescence signals were recorded. Density of Gallyas-positive GCIs in each area is indicated as their number/mm^2. *Black thin bars* indicate relative density for visual comparison. Severity of tissue degeneration (mild moderate or severe) is also shown for each area. None of the items (immunoreactivity to αS or to Ub, density of GCIs) has apparent relation to the severity of lesion or disease duration

stituents of fibrillary structures of LBs and GCIs [32, 38, 39], GCIs are also composed of other proteins [8], such as αB-crystallin, tubulin, tau [30]. In spite of heterogeneous clinical subtypes of MSA (olivopontocerebellar atrophy, striatonigral degeneration and Shy-Drager syndrome) [21, 26], the distribution of GCIs is less heterogeneous, and shared even with advanced cases. This led us to speculate that the evolutionary cascade of each GCI might be relatively homogeneous by undertaking similar steps, whereas degeneration at tissue level is highly variable not necessarily correlated with the frequency of GCIs.

In the present study, we undertook a quantitative analysis on GCIs based on the triple-labeling immunohistochemistry followed by Gallyas silver stain. As previously reported, the prevalence of GCIs in each area in each case has no apparent relationships with the severity of degeneration or the duration of illness [15, 21, 26] as shown in Fig. 3. Our multi-labeling approach demonstrated that αS–Ub+ GCIs were more abundant in cases with longer disease duration (Fig. 4), and its % case-profile was positively correlated with the duration of disease (Fig. 5). Surprisingly, this positive correlation between this % case-profile and the disease duration was found to be perfectly linear (Fig. 5, $R^2=0.983$), in spite of limited number of cases. Furthermore, αS+Ub– GCIs were found to undertake a chronological change reciprocal to αS–Ub+ GCIs, suggesting that αS IR in

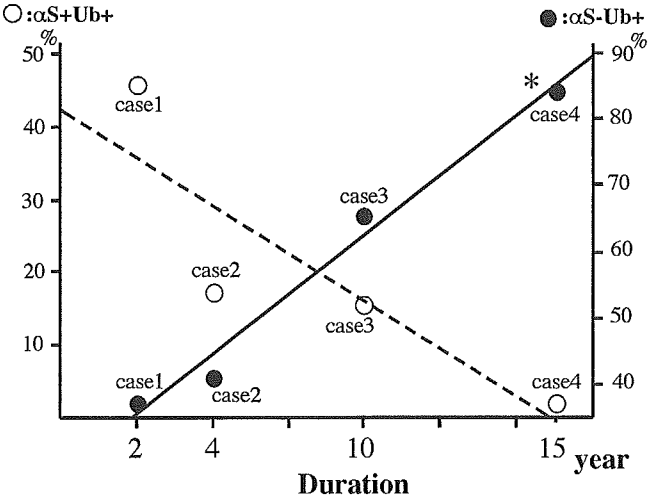

Fig. 5 Regression plot of the relative frequency (% case-profile) of αS–Ub+ (*closed circles*) and that of αS+Ub+ (*open circles*) GCIs in relation to the disease duration. αS–Ub+ GCIs: $R^2=0.983$ $^*P<0.01$; αS+Ub+: $R^2=0.752$

GCIs is being replaced by Ub IR during the disease progression. This contrasting behavior of αS and Ub in GCIs, however, might have been overlooked if one sticks to a single staining profile of GCIs in limited areas. The staining profiles stratified according to the area revealed area-dependent differences, another pos-

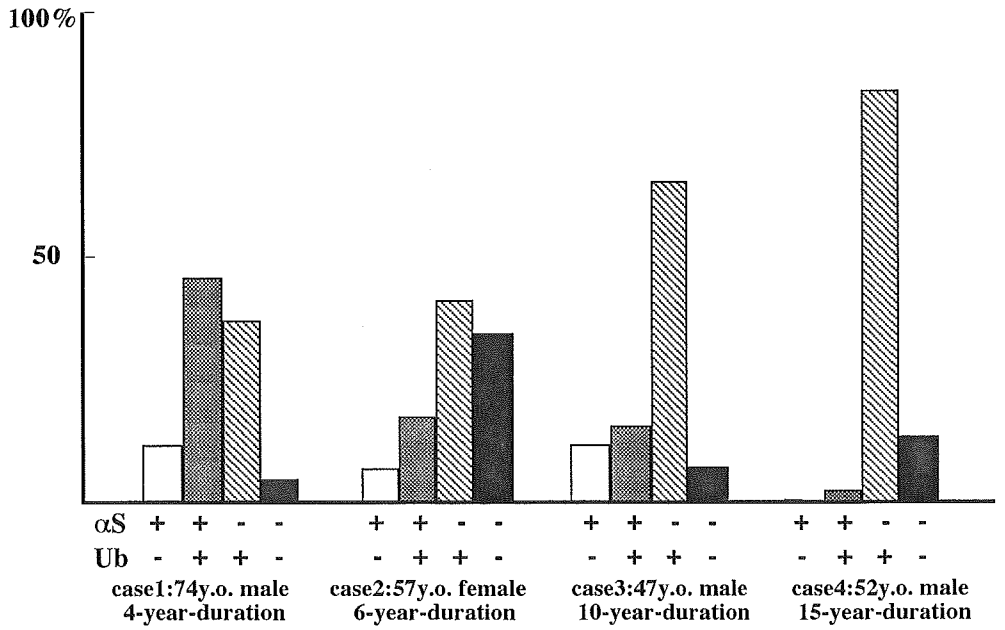

Fig. 4 Differences in the staining profiles of GCIs (% case-profile: a fraction calculated based on the numbers of differently stained GCIs from the three area of each case) with different the disease duration. A progressive increase in αS–Ub+ GCIs and a progressive decrease in αS+Ub+ GCIs with increasing disease duration are apparent. Although this figure is presented with % fractions, case-profile numbers were used for chi-square analyses. The number of αS–Ub+ GCIs was significantly different between cases 4 and 3 ($P<0.0001$), and between cases 3 and 2 ($P<0.0001$). The number of αS+Ub+ GCIs was also significantly different between cases 1 and 2 ($P<0.0001$), and between cases 3 and 4 ($P<0.0001$). Comparison of the number of αS+Ub+ GCIs and that of αS–Ub+ GCIs between cases 2 and 3 by chi-square analysis exhibited no significant difference. The difference was, however, significant between cases 1 and 2 ($P=0.0008$), which was attributable to the relative predominance of αS+Ub+ GCIs in case 1. The opposite predominance of αS–Ub+ GCIs in case 4 relative to case 3 made this difference again significant ($P=0.0001$)

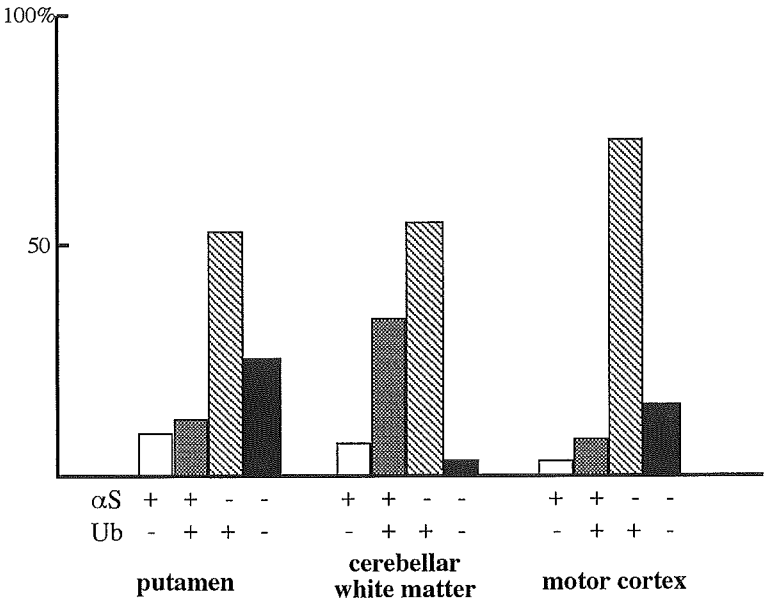

Fig. 6 Different staining profiles of GCIs (% area-profile: a fraction calculated based on the numbers of differently stained GCIs from the same area of the four cases) dependent on the area of interest. Chi-square analyses based on the area-profile numbers demonstrated that cerebellar white matter was characterized by a predominance of αS + Ub + GCIs relative to putamen and motor cortex ($P < 0.0001$). In contrast, motor cortex was characterized by a predominance of αS–Ub + GCIs relative to cerebellar white matter ($P = 0.0016$) and to putamen ($P = 0.0002$)

sible heterogeneity. More interestingly, the abundance of αS–Ub + GCIs, linearly correlated with the disease duration, was characteristics of the motor cortex (Fig. 6). It is suggested that some mechanisms to promote Ub accumulation along with disappearance of αS IR are at work in the advanced stage of this disease. We are, however, still puzzled with this paradox, because lesions of motor cortex in MSA usually remain mild, while GCIs in this area are characterized by the abundance of αS–Ub + GCIs, a feature representative of advanced stage. If the abundance of Ub represents a mechanism that may counteract degenerative process of MSA, it is plausible that its robust expression is related to mild degeneration as seen in the motor cortex.

This progressive decrease in αS IR in GCIs is explained if the target epitope of LB509, that is located to amino acid residues 121/122 of αS [20] is modified or truncated out. Biochemical studies suggest that the filament core of αS (NAC region) has a diameter of 9–10 nm composed of amino acid residues 31–109 of αS [22], whereas GCIs in human brains are composed differently of amorphous material-coated filaments up to 30 nm in diameter. These material-coated filaments consist of 10-nm core fibrils that exhibit a preferential affinity to the antibody against N-terminal 11–26 amino acid residues of αS [9]. It has been reported that formic acid treatment and proteinase K treatment enhance or retrieve LB509 IR in GCIs as well as in aggregated recombinant αS [5, 9, 22]. It is then plausible that progressive accumulation of amorphous material during formation of GCIs may mask some of the αS epitopes. This masking is compatible with the progressive disappearance of αS IR and possibly with progressive accumulation of Ub in GCIs, as we documented in the present study. Otherwise, progressive disappearance of αS may be related to modification of αS itself, possibly different between GCIs and LBs. Immunolabeling with LB509 and some other antibodies against C-terminal and N-terminal epitopes of αS, outside the NAC region, is fainter in GCIs than in LBs [5]. Nitration and phosphorylation seem to be more extensive in GCIs than in LBs [12, 14, 28, 33], although αS in both PD and MSA brains is similarly phosphorylated at Ser-129 and targeted to mono- and di-ubiquitination [7, 13, 25]. Gomez-Tortosa et al. [12] reported that 3-nitrotyrosine (3-NT), a marker of protein nitration through oxidative mechanisms, colocalized with both LBs and GCIs almost equally. Absence of the 3-NT epitope in pale bodies, and nuclear cytoplasmic inclusions in pontine neurons, both recognized by a monoclonal antibody H3C against the C terminus of αS, indicate that nitration is not a prerequisite for αS deposition. We do not yet know, however, whether possible differences between LBs and GCIs detected as some difference in epitope representation of αS or in the extent of nitration suggest distinct cascades for LB and GCI formations or not. Until now, distinction between LBs and GCIs on these immunohistochemical stainings was hardly successful.

In conclusion, multi-labeling of GCIs for αS, Ub, TR and Gallyas silver stain led us to identify a staining profile (αS–Ub +), possibly related to both the duration of disease and to regional preference (a high prevalence of this profile in motor cortex). This is in contrast with cerebellar white matter, where αS + Ub + GCIs are most prevalent. The relevance of GCIs to degeneration remains still obscure. However, identification of these profiles dependent on the area and the disease duration will provide a new cutting edge that may place GCIs and their evolution in a unified framework of degenerative process of MSA.

Acknowledgements We are grateful to Prof. Hiroshi Tanaka and Dr. Michihiko Koeda (Department of Bioinformatics, Medical Research Institute, Tokyo Medical and Dental University) for their help in the statistical analyses. This work was supported in part by the grants from the Ministry of Health and Welfare, Japan (Longevity Science H-14–005 to T.U. and H.M.) and the Ministry

of Education, Culture, Sports, Science and Technology (grant in aid for scientific research B15300118 to T.U.)

References

1. Adams JC (1992) Biotin amplification of biotin and horseradish peroxidase signals in histochemical stains. J Histochem Cytochem 40:1457–1463
2. Baba M, Nakajo S, Tu PH, Tomita T, Nakaya K, Lee VM, Trojanowski JQ, Iwatsubo T (1998) Aggregation of alpha-synuclein in Lewy bodies of sporadic Parkinson's disease and dementia with Lewy bodies. Am J Pathol 152:879–884
3. Braak H, Braak E, Ohm T, Bohl J (1988) Silver impregnation of Alzheimer's neurofibrillary changes counterstained for basophilic material and lipofuscin pigment. Stain Technol 63:197–200
4. Conway KA, Harper JD, Lansbury PT Jr (1998) Accelerated in vitro fibril formation by a mutant alpha-synuclein linked to early-onset Parkinson disease. Nat Med 11:1318–1320
5. Duda JE, Giasson BI, Gur TL, Montine TJ, Robertson D, Biaggioni I, Hurtig HI, Stern MB, Gollomp SM, Grossman M, Lee VM, Trojanowski JQ (2000) Immunohistochemical and biochemical studies demonstrate a distinct profile of alpha-synuclein permutations in multiple system atrophy. J Neuropathol Exp Neurol 59:830–841
6. Fujita T, Doi M, Ogata T, Kanazawa I, Mizusawa H (1993) Cerebral cortical pathology of sporadic olivopontocerebellar atrophy. J Neurol Sci 116:41–46
7. Fujiwara H, Hasegawa M, Dohmae N, Kawashima A, Masliah E, Goldberg MS, Shen J, Takio K, Iwatsubo T (2002) alpha-Synuclein is phosphorylated in synucleinopathy lesions. Nat Cell Biol 4:160–164
8. Gai WP, Power JH, Blumbergs PC, Culvenor JG, Jensen PH (1999) Alpha-synuclein immunoisolation of glial inclusions from multiple system atrophy brain tissue reveals multiprotein components. J Neurochem 73:2093–2100
9. Gai WP, Pountney DL, Power JHT, Li QX, Culvenor JG, McLean CA, Jensen PH, Blumbergs PC (2003) α-Synuclein fibrils constitute the central core of oligodendroglial inclusion filaments in multiple system atrophy. Exp Neurol 181:68–78
10. Giasson BI, Uryu K, Trojanowski JQ, Lee VM (1999) Mutant and wild type human alpha-synucleins assemble into elongated filaments with distinct morphologies in vitro. J Biol Chem 19:7619–7622
11. Goedert M (2001) Alpha-synuclein and neurodegenerative diseases. Nat Rev Neurosci 2:492–501
12. Gomez-Tortosa E, Gonzalo I, Newell K, Garcia YJ, Vonsattel P, Hyman BT (2002) Patterns of protein nitration in dementia with Lewy bodies and striatonigral degeneration. Acta Neuropathol 103:495–500
13. Hasegawa M, Fujiwara H, Nonaka T, Wakabayashi K, Takahashi H, Lee VM, Trojanowski JQ, Mann D, Iwatsubo T (2002) Phosphorylated alpha-synuclein is ubiquitinated in alpha-synucleinopathy lesions. J Biol Chem 13:49071–49076
14. Honjyo Y, Kawamoto Y, Nakamura S, Nakano S, Akiguchi I (2001) P39 immunoreactivity in glial cytoplasmic inclusions in brains with multiple system atrophy. Acta Neuropathol 101:190–194
15. Inoue M, Yagishita S, Ryo M, Hasegawa K, Amano N, Matsushita M (1997) The distribution and dynamic density of oligodendroglial cytoplasmic inclusions (GCIs) in multiple system atrophy: a correlation between the density of GCIs and the degree of involvement of striatonigral and olivopontocerebellar systems. Acta Neuropathol 93:585–591
16. Irizarry MC, Growdon W, Gomez-Isla T, Newell K, George JM, Clayton DF, Hyman BT (1998) Nigral and cortical Lewy bodies and dystrophic nigral neurites in Parkinson's disease and cortical Lewy body disease contain alpha-synuclein immunoreactivity. J Neuropathol Exp Neurol 57:334–337
17. Iwabuchi K, Kosaka K, Haga C, Tuchiya K, Amano N, Itoh K, Yagishita S, Mizutani Y (1991) Study on argyrophilic inclusions of multisystem atrophy. No To Shinkei 43:561–568
18. Iwai A, Masliah E, Yoshimoto M, Ge N, Flanagan L, Silva HA de, Kittel A, Saitoh T (1995) The precursor protein of non-A beta component of Alzheimer's disease amyloid is a presynaptic protein of the central nervous system. Neuron 14:467–475
19. Iwatsubo T, Yamaguchi H, Fujimuro M, Yokosawa H, Ihara Y, Trojanowski JQ, Lee VM (1996) Purification and characterization of Lewy bodies from the brains of patients with diffuse Lewy body disease. Am J Pathol 148:1517–1529
20. Jakes R, Crowther RA, Lee VM-Y, Trojanowski JQ, Iwatsubo T, Goedert M (1999) Epitope mapping of LB509, a monoclonal antibody directed against human alpha-synuclein. Neurosci Lett 269:13–16
21. Lantos PL (1998) The definition of multiple system atrophy: a review of recent developments. J Neuropathol Exp Neurol 57:1099–1111
22. Miake H, Mizusawa H, Iwatsubo T, Hasegawa M (2002) Biochemical characterization of the core structure of alpha-synuclein filaments. J Biol Chem 277:19213–19219
23. Nakazato Y, Yamazaki H, Hirato J, Ishida Y, Yamaguchi H (1990) Oligodendroglial microtubular tangles in olivopontocerebellar atrophy. J Neuropathol Exp Neurol 49:521–530
24. Narhi L, Wood SJ, Steavenson S, Jiang Y, Wu GM, Anafi D, Kaufman SA, Martin F, Sitney K, Denis P, Louis JC, Wypych J, Biere AL, Citron M, (1999) Both familial Parkinson's disease mutations accelerate alpha-synuclein aggregation. J Biol Chem 2:9843–9846
25. Nishie M, Mori F, Fujiwara H, Hasegawa M, Yoshimoto M, Iwatsubo T, Takahashi H, Wakabayashi K (2004) Accumulation of phosphorylated alpha-synuclein in the brain and peripheral ganglia of patients with multiple system atrophy. Acta Neuropathol 107:292–298
26. Papp MI, Lantos PL (1994) The distribution of oligodendroglial inclusions in multiple system atrophy and its relevance to clinical symptomatology. Brain 117:235–243
27. Papp MI, Kahn JE, Lantos PL (1989) Glial cytoplasmic inclusions in the CNS of patients with multiple system atrophy (striatonigral degeneration, olivopontocerebellar atrophy and Shy-Drager syndrome). J Neurol Sci 94:79–100
28. Piao YS, Hayashi S, Hasegawa M, Wakabayashi K, Yamada M, Yoshimoto M, Ishikawa A, Iwatsubo T, Takahashi H (2001) Co-localization of alpha-synuclein and phosphorylated tau in neuronal and glial cytoplasmic inclusions in a patient with multiple system atrophy of long duration. Acta Neuropathol 101:285–293
29. Sakamoto M, Uchihara T, Hayashi M, Nakamura A, Kikuchi E, Mizutani T, Mizusawa H, Hirai S (2002) Heterogeneity of nigral and cortical Lewy bodies differentiated by amplified triple-labeling for alpha-synuclein, ubiquitin, and thiazin red. Exp Neurol 177:88–94
30. Shibuya K, Uchihara T, Nakamura A, Ishiyama M, Yamaoka K, Yagishita S, Iwabuchi K, Kosaka K (2003) Reversible conformational change of tau2 epitope on exposure to detergent in glial cytoplasmic inclusions of multiple system atrophy. Acta Neuropathol 105:508–514
31. Spillantini MG, Schmidt ML, Lee VM, Trojanowski JQ, Jakes R, Goedert M (1997) Alpha-synuclein in Lewy bodies. Nature 28:839–840
32. Spillantini MG, Crowther RA, Jakes R, Cairns NJ, Lantos PL, Goedert M (1998) Filamentous alpha-synuclein inclusions link multiple system atrophy with Parkinson's disease and dementia with Lewy bodies. Neurosci Lett 251:205–208
33. Takahashi M, Iseki E, Kosaka K (2000) Cyclin-dependent kinase 5 (Cdk5) associated with Lewy bodies in diffuse Lewy body disease. Brain Res 862:253-256
34. Tu PH, Galvin JE, Baba M, Giasson B, Tomita T, Leight S, Nakajo S, Iwatsubo T, Trojanowski JQ, Lee VM (1998) Glial cytoplasmic inclusions in white matter oligodendrocytes of multiple system atrophy brains contain insoluble alpha-synuclein. Ann Neurol 44:415–422

35. Uchihara T, Nakamura A, Nagaoka U, Yamazaki M, Mori O (2000) Dual enhancement of double immunofluorescent signals by CARD: participation of ubiquitin during formation of neurofibrillary tangles. Histochem Cell Biol 114:447–451
36. Uchihara T, Nakamura A, Yamazaki M, Mori O (2000) Tau-positive neurons in corticobasal degeneration and Alzheimer's disease—distinction by thiazin red and silver impregnations. Acta Neuropathol 100:385–389
37. Uchihara T, Nakamura A, Nakayama H, Arima K, Ishizuka N, Mori H, Mizushima S (2003) Triple immunofluorolabeling with two rabbit polyclonal antibodies and a mouse monoclonal antibody allowing three-dimensional analysis of cotton wool plaques in Alzheimer disease. J Histochem Cytochem 51:1201–1206
38. Wakabayashi K, Hayashi S, Kakita A, Yamada M, Toyoshima Y, Yoshimoto M, Takahashi H (1998) Accumulation of alpha-synuclein/NACP is a cytopathological feature common to Lewy body disease and multiple system atrophy. Acta Neuropathol 96:445-452
39. Wakabayashi K, Yoshimoto M, Tsuji S, Takahashi H, (1998) Alpha-synuclein immunoreactivity in glial cytoplasmic inclusions in multiple system atrophy. Neurosci Lett 19:180–182

Available online at www.sciencedirect.com
SCIENCE DIRECT®
Analytical Biochemistry 347 (2005) 106–111
ANALYTICAL BIOCHEMISTRY
www.elsevier.com/locate/yabio

More than a 100-fold increase in immunoblot signals of laser-microdissected inclusion bodies with an excessive aggregation property by oligomeric actin interacting protein 2/D-lactate dehydrogenase protein 2

Naomi S. Hachiya [a], Takuya Ohkubo [b], Yoshimichi Kozuka [c], Mineo Yamazaki [d], Osamu Mori [e], Hidehiro Mizusawa [b], Yuji Sakasegawa [f], Kiyotoshi Kaneko [a,*]

[a] *Second Department of Physiology, Tokyo Medical University, Shinjuku-ku, Tokyo 160-8402, Japan*
[b] *Department of Neurology and Neurological Science, Graduate School of Medicine, Tokyo Medical and Dental University, Bunkyo-ku, Tokyo 113-0034, Japan*
[c] *Ultrastructural Research, National Institute of Neuroscience, National Center of Neurology and Psychiatry, Kodaira, Tokyo 187-8502, Japan*
[d] *Department of Neurology and Nephrology, Nippon Medical School, Bunkyo-ku, Tokyo 113-8602, Japan*
[e] *Second Department of Pathology, Nippon Medical School, Bunkyo-ku, Tokyo 113-8602, Japan*
[f] *Division of Prion Protein Biology, Department of Prion Protein Research, Graduate School of Medicine, Tohoku University, Aoba-ku, Sendai 980-8575, Japan*

Received 6 July 2005
Available online 26 September 2005

Abstract

We established a histobiochemical approach targeting micron-order inclusion bodies possessing extensive aggregation properties in situ by using a nonchemical denaturant (oligomeric actin interacting protein 2/D-lactate dehydrogenase protein 2 [Aip2p/Dld2p]) with the combinatorial method of laser-microdissection and immunoblot analysis. As a model, pick bodies were chosen and laser-microdissected from three different brain regions of two patients with Pick's disease. Initially, 500 to 2000 pick bodies were applied onto SDS–PAGE gels after boiling in Laemmli's sample buffer according to established immunoblotting procedures; however, only faint signals were obtained. Following negative results with chemical denaturants or detergent, including 6 M guanidine hydrochloride, 8 M urea, and 2% SDS, the laser-microdissected pick bodies were pretreated with oligomeric Aip2p/Dld2p, which possesses robust protein unfolding activity under biological conditions. Strikingly, only one pick body was sufficient to illustrate an immunoblot signal, indicating that pretreatment with oligomeric Aip2p/Dld2p enhanced the immunoblot sensitivity by more than 100-fold. Pretreatment with oligomeric Aip2p/Dld2p also allowed us to quantify the total protein content of pick bodies. Thus, use of oligomeric Aip2p/Dld2p significantly contributed toward the acquisition of information pertaining to the molecular profile of proteins possessing an extensive aggregation property, particularly in small amounts.

Keywords: Oligomeric Aip2p/Dld2p; Protein conformation unfolding activity; Laser-microdissection; Inclusion bodies; Pick bodies; Phosphorylated tau

While immunohistochemical analysis has been widely used for the characterization of microstructures under various conditions and of disorders at a light microscopic level, immunoblot analysis has been indispensable in the analysis of proteins at a macroscopic level [1]. Currently, no analytical methods equivalent to the immunoblot have been developed against targets for examination under the microscope, although the recent development of a laser-microdissection methodology allows us to manipulate microstructures at microscopic regions of interest in situ [2].

* Corresponding author. Fax: +81 3 3351 6544.
E-mail address: k-kaneko@tokyo-med.ac.jp (K. Kaneko).

0003-2697/$ - see front matter © 2005 Elsevier Inc. All rights reserved.
doi:10.1016/j.ab.2005.09.004

Against this backdrop, we developed a novel combinatorial method that uses laser-microdissection and immunoblotting to allow the characterization of the molecular profile of proteins at microscopic regions of interest. As a model, we examined brain samples of Pick's disease, a type of progressive presenile dementia that affects brain function, eventually causing loss of verbal skills and problem-solving ability [3]. Pick's disease accounts for 5% of all dementias and is characterized neuropathologically by distinct tau-immunoreactive intraneuronal inclusions known as pick bodies [4]. Abnormally phosphorylated tau proteins were detected from total brain homogenates [4–6], but no investigation has been reported with isolated pick bodies to date.

Given limited sample availability and the absence of in vitro amplification steps for proteins, use of laser-microdissected samples depends largely on highly sensitive protein detection methods [7]. Furthermore, these inclusion bodies generally possess extensive aggregation properties that often negatively affect the immunoblot assay. Unfortunately, use of conventional procedures, including sample pretreatment with chemical denaturing agents or detergent, was ineffective. In an effort to overcome the problem, oligomeric actin interacting protein 2 (Aip2p)[1] [8]/D-lactate dehydrogenase protein 2 (Dld2p) [9,10] was used as a non-chemical denaturant [11–13]. Dld2p [9,10] was initially identified as Aip2p using a two-hybrid screen to search for proteins that interact with actin [8]. During our search for protein conformation unfolding activity, we further identified oligomeric Aip2p/Dld2p isolated from *Saccharomyces cerevisiae* as exhibiting robust protein conformation unfolding activity [11]. Oligomeric Aip2p/Dld2p possesses a unique grapple-like structure with an ATP-dependent opening that is required for protein conformation unfolding activity [12,13]. In the presence of 1 mM ATP or AMP–PNP, oligomeric Aip2p/Dld2p bound to all substrates so far examined and subsequently modified the protein conformation. Furthermore, oligomeric Aip2p/Dld2p was able to modify the conformation of pathogenic highly aggregated polypeptides such as recombinant prion protein (rPrP) in the beta form, alpha-synuclein, and Abeta (1–42) in the presence of ATP in vitro [13]. This procedure consists simply of combining oligomeric Aip2p/Dldp2 and 1 mM ATP in a reaction tube containing the collected pick bodies and then incubating the sample for 60 min at 30 °C.

Oligomeric Aip2p/Dld2p significantly increases the immunoblot signals by more than 100-fold. The histobiochemical approach detailed in this study allows us to analyze single pick bodies in the order of several micrometers in radius.

[1] *Abbreviations used*: Aip2p, actin interacting protein 2; Dld2p, D-lactate dehydrogenase protein 2; rPrP, recombinant prion protein; BSA, bovine serum albumin; EGTA, ethyleneglycotetraacetic acid; TCA, trichloroacetic acid; PBS, phosphate-buffered saline; PBS-T, PBS containing 0.05% Tween 20; TBH, total brain homogenate; LC–MS/MS, liquid chromatography–tandem mass spectrometry.

Materials and methods

After informed consent had been obtained, frontal (Y337F and Y332F) and temporal (Y332T) cortexes from two patients with sporadic Pick's disease (patient 1 (Y337): female, 71 years old; patient 2 (Y332): male, 72 years old) were placed in a deep freezer (−80 °C) at Nippon Medical School until use. The procedures followed were in accordance with the institutional ethical standards on human experimentation.

Oligomeric Aip2p/Dld2p was expressed and purified as described previously [11,12]. Anti-tau AT8 (phosphorylation-dependent monoclonal antibody specific to phosphorylated Ser202/Thr205) and AT100 (specific to phosphorylated Thr212/Ser214) were purchased from Innogenetics. Anti-Aip2p/Dld2p antibody was raised against the synthetic peptide corresponding to the C-terminal 15 amino acid residues of Aip2p (VHYDPNGILNPYKYI) that were coupled through a COOH-terminal cysteine residue to bovine serum albumin (BSA) [11].

Slide preparations were made using a NexES Automated Immunohistochemistry Staining System (Ventana Medical Systems) with 1:200 AT8. Immunostained pick bodies (10–15 μm in diameter) (Table 1) were dissected using a Laser Microdissection System (Olympus Optical) coupled to a Hoya laser cutter (HCL2100, 30 mJ/pulse, 266 nm). Dissected samples were collected using a Cell Tram Oil hydraulic manual microinjector (Eppendorf) with distilled water.

Immunoblot analyses were performed as follows. First, total brain homogenates (10–40 μg) or laser-dissected pick bodies (500 pieces) were solubilized in 500 μl of ice-cold extraction buffer (Tris–chloride [pH 7.4], 0.8 M NaCl, 1 mM ethyleneglycotetraacetic acid [EGTA], 10% sucrose, and 1/1000 [w/v] protease inhibitor cocktail [Sigma] with 1% sodium *N*-lauroyl sarcosinate [sarkosyl]). Sarkosyl-insoluble fractions were collected by centrifugation at 182,000*g* for 30 min at 4 °C and then suspended in 50 mM Tris–chloride (pH 7.4). Samples were pretreated with 8 M urea (Wako Chemicals), 6 M guanidine hydrochloride (Nacalai Tesque), or 2% SDS (Wako Chemicals), followed by trichloroacetic acid (TCA) precipitation in an effort to denature or untangle the samples. Pretreatment with Aip2p/Dld2p was performed as described previously

Table 1
Quantitative analyses of pick bodies

	Y332T	Y332F	Y337F
Total protein (ng/pick body)	0.8	1.1	2.8
Average diameter (μm)	10	10	15
SRelative density	1.6	2.2	1.6

Note. The protein concentration of sarkosyl-insoluble fractions was measured following pretreatment with oligomeric Aip2p/Dld2p, and the relative density of the pick bodies was calculated. Frontal (Y337F and Y332F) and temporal (Y332T) cortexes from two patients with sporadic Pick's disease (patient 1 (Y337): female, 71 years old; patient 2 (Y332): male, 72 years old) were analyzed.

[11–13]. Briefly, 1 to 500 ng of oligomeric Aip2p/Dld2p was mixed with the sarkosyl-insoluble fraction of 1 to 500 pick bodies at a ratio of 1 ng per 1 pick body in the presence of 1 mM ATP for 60 min at 30 °C in a total volume of 20 μl. Samples were then loaded onto 12% SDS–PAGE gels and transferred onto 0.22-μm nitrocellulose membranes in 25 mM Tris–190 mM glycine–0.01% SDS–20% methanol at 400 mA for 40 min at 4 °C. Membranes were blocked using 4% BSA in phosphate-buffered saline (PBS) containing 0.05% Tween 20 (PBS-T), incubated with 1:1000 (unless otherwise indicated) AT8 and AT100 in PBS-T overnight at 4 °C, washed with PBS-T several times at room temperature, and then incubated with 1:10,000 horseradish peroxidase-conjugated anti-mouse IgG antibody (Amersham) in PBS-T for 1 h at room temperature. After washing the membranes, the immunodecorated bands were visualized using ECL-plus (Amersham) and then analyzed using a Fluor-S MAX MultiImager or VersaDoc (Bio-Rad Laboratories).

The protein concentration of the pick bodies pretreated with oligomeric Aip2p/Dld2p was measured using a spectrophotometer (Tecan) at 595 nm in combination with a Protein Assay System (Bio-Rad Laboratories) according to the manufacturers' instructions. Oligomeric Aip2p/Dld2p was applied at a ratio of 1 ng per 1 pick body, and the value was subtracted afterward.

Results

The laser-microdissection system combined with the sample collector facilitated the dissection of targets (Fig. 1A). Up to 500 pick bodies were collected each time over a period of 1 day. Initially, 500 pick bodies were applied onto SDS–PAGE gels after boiling in Laemmli's sample buffer according to established immunoblotting procedures [1]. However, only faint and blurred signals were obtained with anti-tau antibodies AT8 and AT100 (Fig. 1B, lane 4) in comparison with 10 to 40 μg of total brain homogenate (TBH, Fig. 1B, lanes 2 and 3). Immunostaining of the entire gel, including the loading wells and the stacking gel, revealed no additional immunoblot signals that may have arisen from the extensive aggregation property of the pick bodies. Further increases in the number of pick bodies applied (up to 2000) could not improve the signal intensity (data not shown).

The effect of chemical denaturants or detergent, including 6 M guanidine hydrochloride, 8 M urea, and 2% SDS,

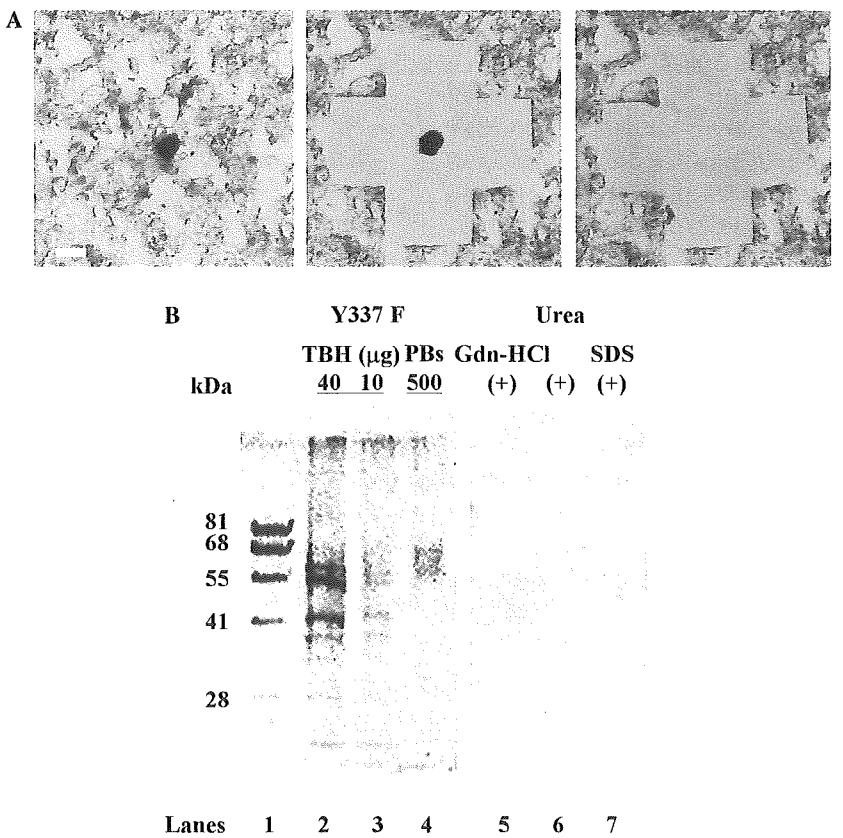

Fig. 1. Immunological analyses of laser-microdissected pick bodies (PBs). (A) Left panel: 5-μm-thick cryosection. PBs of frontal cortex from patient Y337 (Y337F) are stained with AT8 (1:200, purple) and hematoxylin (blue). Middle and right panels: PBs isolated from the section using a laser-microdissector. Scale bar is 10 μm. (For interpretation of the references to color in this figure legend, the reader is referred to the Web version of this article.) (B) Immunoblot analyses of PBs pretreated with chemical denaturants or detergent. Approximately 500 PBs were used for each trial. Lane 1: molecular weight marker (Dr. Western, Oriental Yeast); lanes 2 and 3: total brain homogenate (TBH) of Y337F (40 and 10 μg, respectively); lanes 4 to 7: 500 laser-microdissected PBs of Y337F with no pretreatment (lane 4), 6 M guanidine hydrochloride (Gdn-HCl, lane 5), 8 M urea (lane 6), and 2% SDS pretreatment (lane 7). Samples were stained with anti-tau AT8 (1:1000) and AT100 (1:1000).

was then determined. Use of the aforementioned chaotropic agents, however, resulted in no improvement of immunoblot signals (Fig. 1B, lanes 5–7). In fact, the signal intensities diminished somewhat, possibly due to the presence of phosphorylated tau bound to the walls of the tube after removing the chaotropic agents prior to loading onto the SDS–PAGE gels [14].

Although negative results were obtained following use of the aforementioned chemical denaturants and detergent, we demonstrated that oligomeric Aip2p/Dld2p could modify the conformation of pathogenic highly aggregated polypeptides such as rPrP in the beta form, alpha-synuclein, and Abeta (1–42) in the presence of ATP [13]. Hence, the pick bodies were pretreated with oligomeric Aip2p/Dld2p prior to loading onto SDS–PAGE gels. Surprisingly, immunoblot analyses of Y337F, Y332F, and Y332T demonstrated discrete bands stained with anti-tau AT8 and AT100 antibodies following pretreatment with oligomeric Aip2p/Dld2p (Fig. 2). In a serial dilution assay, 1/500 of 500 pick bodies (equivalent to 1 pick body) was detected (Fig. 2, upper panel, lanes 4–8; lower panel, lanes 2–10).

These immunoreactive bands migrated slightly faster than those associated with the 500 pick bodies processed without oligomeric Aip2p/Dld2p pretreatment (Fig. 2, upper panel, lane 2). One possible explanation is that pretreatment with oligomeric Aip2p/Dld2p might allow the detection of the phosphorylated form of 60 kDa tau (tau 60) [4–6], whereas only the phosphorylated form of 69 kDa tau (tau 69) is negligibly detected following boiling in Laemmli's sample buffer according to classical immunoblotting procedures. Whether the different tau isoform could account for the faster migration pattern observed remains to be determined.

Oligomeric Aip2p/Dld2p was also detected in the same reaction mixtures using anti-Aip2p/Dld2p antibody (Fig. 2, upper panel, lanes 12–16) but did not cross-react with anti-tau AT8 and AT100 antibodies (Fig. 2, upper panel, lane 10). It should be noted that a single pick body directly pretreated with oligomeric Aip2p/Dld2p was sufficient to yield an immunoblot signal (Fig. 2, lower panel, lane 13), indicating that pretreatment with oligomeric Aip2p/Dld2p enhanced the immunoblot signal by more than 100-fold. Transmission electron microscopy with uranyl acetate negative staining of laser-microdissected pick bodies (Fig. 3) revealed that they were untangled following treatment with oligomeric Aip2p/Dld2p, whereas the

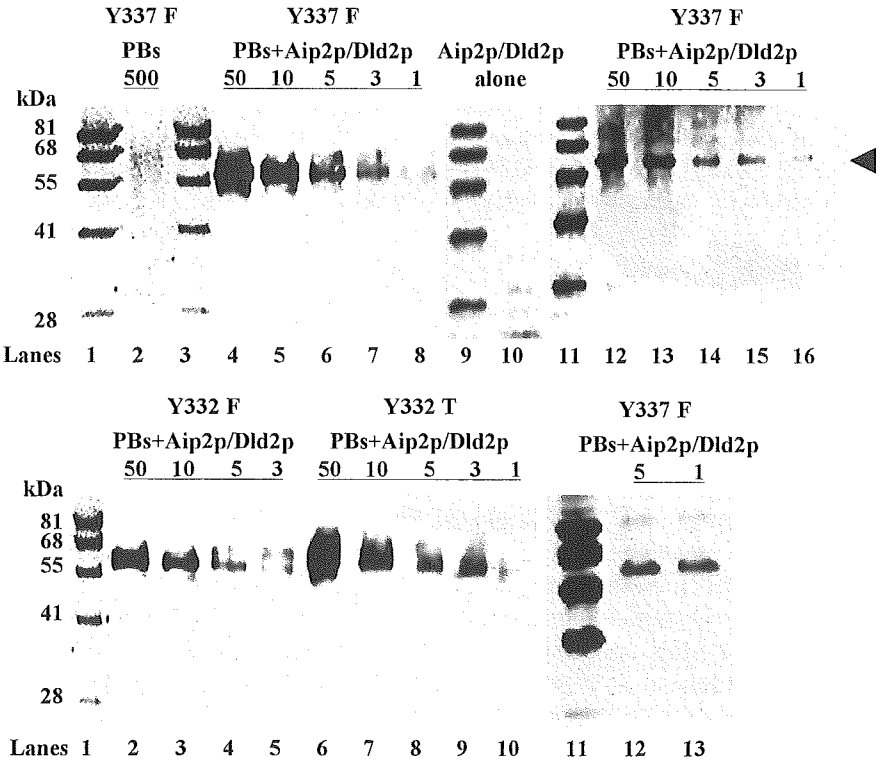

Fig. 2. Immunoblot analyses of laser-microdissected pick bodies (PBs) from Y337F (frontal cortex), Y332F (frontal cortex), and Y332T (temporal cortex). Upper panels: Molecular weight marker (Dr. Western, Oriental Yeast, lanes 1, 3, 9, and 11), 500 laser-microdissected PBs of Y337F (lane 2), and serial dilutions equivalent to 50, 10, 5, and 3 PBs and 1 PB of Y337F (lanes 4–8 and 12–16). Lane 2 represents sample without oligomeric Aip2p/Dld2p pretreatment, whereas lanes 4 to 8 and lanes 12 to 16 represent samples with oligomeric Aip2p/Dld2p pretreatment. Lane 10: 50 ng of Aip2p/Dld2p alone. Lanes 2, 4 to 8, and 10 were stained with anti-tau AT8 (1:1000) and AT100 (1:1000), whereas lanes 12 to 16 were stained with anti-Aip2p/Dld2p polyclonal antibody. The arrowhead indicates the position of Aip2p/Dld2p (MW = 58 kDa). Lower panels: Molecular weight marker (Dr. Western, Oriental Yeast, lanes 1 and 11), serial dilutions of 500 PBs of Y332F equivalent to 50, 10, 5, and 3 PBs (lanes 2–5), and those of Y332T equivalent to 50, 10, 5, and 3 PBs and 1 PB (lanes 6–10). Lanes 12 and 13: 5 PBs and 1 PB of Y337F, respectively. Samples in lower panels were pretreated with oligomeric Aip2p/Dld2p and stained with anti-tau AT8 (1:1000) and AT100 (1:1000).

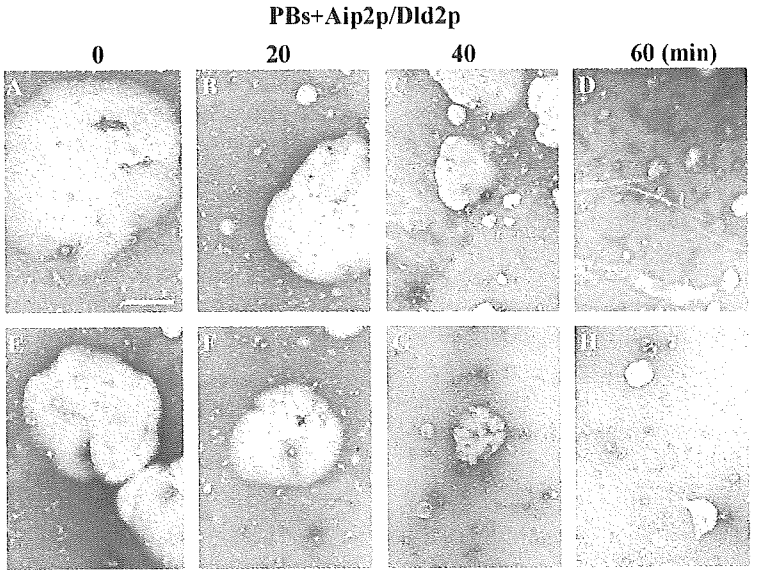

Fig. 3. Transmission electron microscopy with uranyl acetate negative staining of laser-microdissected pick bodies (PBs) prior to (A and E) and following oligomeric Aip2p/Dld2p pretreatment for 20 min (B and F), 40 min (C and G), and 60 min (D and H). For the negative staining, 500 PBs of Y332F were used as specimens. Scale bar is 4 μm.

average diameter of pick bodies decreased markedly, from 10 to 15 μm to less than 1 μm, in a time-dependent manner.

Although protein quantification of highly aggregated proteins such as pick bodies has been quite problematic to date, pretreatment with oligomeric Aip2p/Dld2p allows the ready quantification of the protein content of pick bodies (Table 1). The protein concentrations of sarkosyl-insoluble fractions were 0.8 ng (Y332T), 1.1 ng (Y332F), and 2.8 ng (Y337F) per 1 pick body. Because the average diameters of the pick bodies were 10 μm (Y332) and 15 μm (Y337), the relative densities of the pick bodies were 1.6 to 2.2 (Y332) and 1.6 (Y337).

Discussion

Our novel combinatorial method targets proteins relating to specific regions of interest at the micrometer order and exclusively allows the gathering of information pertaining to the molecular profile, such as molecular weight, of target proteins under the microscope in situ. During our investigations, we noticed that laser-microdissected pick bodies exhibited only faint and blurred immunoblot signals with anti-tau AT8 and AT100 antibodies, even following pretreatment with chemical denaturants or detergent, presumably resulting from the extensive aggregation property. In fact, this is extremely crucial when only a minimal quantity of target protein is available.

The protein conformation unfolding activity of oligomeric Aip2p/Dld2p can modify the conformation of pathogenic highly aggregated polypeptides [13]. Therefore, pick bodies were pretreated with oligomeric Aip2p/Dld2p to overcome the extensive aggregation property. With the pretreatment, 500 ng of oligomeric Aip2p/Dld2p (MW ~700 kDa) was mixed with 500 pick bodies consisting of abnormally phosphorylated tau (MW = 58 kDa), indicating that the stoichiometry of oligomeric Aip2p/Dld2p:phosphorylated tau is approximately 1:10. As shown in Fig. 2, oligomeric Aip2p/Dld2p pretreatment enhanced the immunoblot signals by more than 100-fold.

The inclusion bodies, which might protect against toxicity [15], have been associated with various protein conformation disorders, including Alzheimer's disease [16], Parkinson's disease [17], and prion disease (e.g., bovine spongiform encephalopathy) [18]. Actually, the robust protein conformation unfolding activity of oligomeric Aip2p/Dld2p modulated the conformation of Abeta (1–42) peptide associated with Alzheimer's disease, alpha-synuclein associated with Parkinson's disease, and rPrP in the beta form associated with prion disease in vitro [13]. Therefore, use of oligomeric Aip2p/Dld2p with our combinatorial method provides significant improvement in the investigation of normal or abnormal microstructures under various conditions and of disorders with extremely enhanced sensitivity.

Making use of this unprecedented property of oligomeric Aip2p/Dld2p may yield further potential applications. For example, a number of proteomic strategies rely on liquid chromatography–tandem mass spectrometry (LC–MS/MS), but sample preparation methods typically involve the use of detergents and chaotropic agents that often interfere with chromatographic separation and/or electrospray ionization [19]. Use of oligomeric Aip2p/Dld2p, however, would not interfere with the LC–MS/MS procedures and might even prove to be ideal for sample pretreatment. Overall, use of oligomeric Aip2p/Dld2p might significantly facilitate nano-scale analysis, which is often hindered by the aggregation property of target proteins present under various analytical conditions, especially when the sample protein is present in minor quantities.

Acknowledgments

We thank K. Watanabe and K. Takayama for technical assistance. This work was supported by grants from the Ministry of Health, Labor, and Welfare and the Ministry of Education, Culture, Sports, Science, and Technology, Japan, and from the Core Research for Evolutional Science and Technology (CREST) of Japan Science and Technology Agency.

References

[1] U.K. Laemmli, Cleavage of structural proteins during the assembly of the head of bacteriophage T4, Nature 227 (1970) 680–685.
[2] T. Tanaka, T. Ito, M. Furuta, C. Eguchi, H. Toda, E. Wakabayashi-Takai, K. Kaneko, In situ phage screening: a method for identification of subnanogram tissue components in situ, J. Biol. Chem. 277 (2002) 30382–30387.
[3] S. Hardin, B. Schooley, A story of Pick's disease: a rare form of dementia, J. Neurosci. Nurs. 34 (2002) 117–122.
[4] V. Zhukareva, D. Mann, S. Pickering-Brown, K. Uryu, T. Shuck, K. Shah, M. Grossman, B.L. Miller, C.M. Hulette, S.C. Feinstein, J.Q. Trojanowski, V.M. Lee, Sporadic Pick's disease: a tauopathy characterized by a spectrum of pathological tau isoforms in gray and white matter, Ann. Neurol. 51 (2002) 730–739.
[5] A. Delacourte, N. Sergeant, A. Wattez, D. Gauvreau, Y. Robitaille, Vulnerable neuronal subsets in Alzheimer's and Pick's disease are distinguished by their tau isoform distribution and phosphorylation, Ann. Neurol. 43 (1998) 193–204.
[6] T. Arai, K. Ikeda, H. Akiyama, Y. Shikamoto, K. Tsuchiya, S. Yagishita, T. Beach, J. Rogers, C. Schwab, P.L. McGeer, Distinct isoforms of tau aggregated in neurons and glial cells in brains of patients with Pick's disease, corticobasal degeneration, and progressive supranuclear palsy, Acta Neuropathol. (Berl.) 101 (2001) 167–173.
[7] W. Martinet, V. Abbeloos, N. Van Acker, G.R. De Meyer, A.G. Herman, M.M. Kockx, Western blot analysis of a limited number of cells: a valuable adjunct to proteome analysis of paraffin wax-embedded, alcohol-fixed tissue after laser capture microdissection, J. Pathol. 202 (2004) 382–388.
[8] D.C. Amberg, E. Basart, D. Botstein, Defining protein interactions with yeast actin in vivo, Nat. Struct. Biol. 2 (1995) 28–35.
[9] A. Chelstowska, Z. Liu, Y. Jia, D. Amberg, R.A. Butow, Signalling between mitochondria and the nucleus regulates the expression of a new D-lactate dehydrogenase activity in yeast, Yeast 15 (1999) 1377–1391.
[10] M.J. Flick, S.F. Konieczny, Identification of putative mammalian D-lactate dehydrogenase enzymes, Biochem. Biophys. Res. Commun. 295 (2002) 910–916.
[11] N.S. Hachiya, Y. Sakasegawa, A. Jozuka, S. Tsukita, K. Kaneko, Interaction of D-lactate dehydrogenase protein 2 (Dld2p) with F-actin: Implication for an alternative function of Dld2p, Biochem. Biophys. Res. Commun. 319 (2004) 78–82.
[12] N.S. Hachiya, Y.H.S. Sakasegawa, A. Jozuka, S. Tsukita, K. Kaneko, Oligomeric Aip2p/Dld2p forms a novel grapple-like structure and has an ATP-dependent F-actin conformation modifying activity in vitro, Biochem. Biophys. Res. Commun. 320 (2004) 1271–1276.
[13] N.S. Hachiya, Y.H.S. Sakasegawa, A. Jozuka, S. Tsukita, K. Kaneko, Oligomeric Aip2p/Dld2p modifies the protein conformation of both properly-folded and misfolded substrates in vitro, Biochem. Biophys. Res. Commun. 323 (2004) 339–344.
[14] K. Kaneko, D. Peretz, K.M. Pan, T.C. Blochberger, H. Wille, R. Gabizon, O.H. Griffith, F.E. Cohen, M.A. Baldwin, S.B. Prusiner, Prion protein (PrP) synthetic peptides induce cellular PrP to acquire properties of the scrapie isoform, Proc. Natl. Acad. Sci. USA 92 (1995) 11160–11164.
[15] M. Tanaka, Y.M. Kim, G. Lee, E. Junn, T. Iwatsubo, M.M. Mouradian, Aggresomes formed by alpha-synuclein and synphilin-1 are cytoprotective, J. Biol. Chem. 279 (2004) 4625–4631.
[16] J.W. Lustbader, M. Cirilli, C. Lin, H.W. Xu, K. Takuma, N. Wang, C. Caspersen, X. Chen, S. Pollak, M. Chaney, F. Trinchese, S. Liu, F. Gunn-Moore, L.F. Lue, D.G. Walker, P. Kuppusamy, Z.L. Zewier, O. Arancio, D. Stern, S.S. Yan, H. Wu, ABAD directly links Abeta to mitochondrial toxicity in Alzheimer's disease, Science 304 (2004) 448–452.
[17] J.T. Greenamyre, T.G. Hastings, Parkinson's: divergent causes, convergent mechanisms, Science 304 (2004) 1120–1122.
[18] M.P. Mayer, H. Schroder, S. Rudiger, K. Paal, T. Laufen, B. Bukau, Multistep mechanism of substrate binding determines chaperone activity of Hsp70, Nat. Struct. Biol. 7 (2000) 586–593.
[19] J. Blonder, M.B. Goshe, R.J. Moore, L. Pasa-Tolic, C.D. Masselon, M.S. Lipton, R.D. Smith, Enrichment of integral membrane proteins for proteomic analysis using liquid chromatography–tandem mass spectrometry, J. Proteome Res. 1 (2002) 351–360.